Research Square

Preprints are preliminary reports that have not undergone peer review.
They should not be considered conclusive, used to inform clinical practice,
or referenced by the media as validated information.

Label-free biocompatible detection and quantification of airborne particulate matter (PM2.5) and chronic tissue injury in heart and lung of mouse

Saira Hameed
Department of Chemistry, Umeå University
Kun Pan
Department of Environmental Health, School of Public Health and the Key Laboratory of Public Health Safety, Ministry of Education, Fudan University
Wenhua Su
Department of Optical Science and Engineering, Fudan University
Miles Trupp
Department of Clinical Neurosciences, Umeå University
Lan Mi
Department of Optical Science and Engineering, Fudan University
Jinzhuo Zhao (jinzhuozhao@fudan.edu.cn)
Department of Environmental Health, School of Public Health and the Key Laboratory of Public Health Safety, Ministry of Education, Fudan University

Research Article

Keywords: Fluorescence lifetime imaging microscopy (FLIM), Field emission scanning electron microscopy (FE-SEM), PM2.5, Heart, Lung, Injury

Posted Date: April 12th, 2022

DOI: https://doi.org/10.21203/rs.3.rs-1503565/v1

License: This work is licensed under a Creative Commons Attribution 4.0 International License.
Read Full License

Abstract

While it is known that air borne particulate matter ($PM_{2.5}$) may pass through the pulmonary circulation of blood at the alveolar level between lung and heart and cross the air-blood barrier, the mechanism and effects are not completely clear. In this study the imaging method fluorescence lifetime imaging microscopy (FLIM) is adopted for visualization with high spatial resolution and quantification of PM particles in mouse lung and heart tissues. The results showed that the median numbers of particles in lung of mice exposed to particulate matter of diameter less than 2.5 μm ($PM_{2.5}$) was about 2.0 times more than that in the filtered air (FA)-treated mice, and about 1.3 times more in heart of $PM_{2.5}$-treated mice than in FA-treated mice. Interestingly, $PM_{2.5}$ particles were more abundant in heart than lung, likely due to how PM particles are cleared by phagocytosis and transport via circulation from lungs. It is proposed that the powerful flow of blood through the heart may contribute to invasion of $PM_{2.5}$ particles into heart muscles. The histopathological evaluations revealed that exposure of $PM_{2.5}$ to lungs dilated air spaces and showed signs of inflammation. Moreover, heart tissues showed inflammation and amyloid deposition. The component analysis of concentrated airborne $PM_{2.5}$ particles suggested traffic exhausts and industrial emissions as predominant sources. Our results strongly suggest association of $PM_{2.5}$ exposure to chronic lung and heart tissue injuries. The current study supports the contention that industrial air pollution is one of the causative factors for rising levels of chronic pulmonary and cardiac diseases.

Introduction

Air borne particulate matter less than 2.5 μm in size ($PM_{2.5}$) is the leading environmental risk factor that impairs metabolic homeostasis [1], and is associated with the morbidity and mortality of cardiopulmonary diseases [2]. Sixteen mice were divided into two groups and were exposed to concentrated $PM_{2.5}$ (PM, dirty air), and filtered air (FA, control), using the “Shanghai Meteorological and Environmental Animal Exposure System (Shanghai-METAS)”, located in the School of Public Health at Fudan University at Xujiahui District in Shanghai. Air borne $PM_{2.5}$ directly enters into the lungs by inhalation and is transported into extrapulmonary organs such as kidney, and liver, [3], including brain [4]. The quantification of $PM_{2.5}$ particles can contribute to elucidation of the effects of $PM_{2.5}$ on different tissues and organs. Previous studies have shown a correlation between the amount of brain magnetite and the incidence of Alzheimer’s disease [5, 6]. Our previous study has shown that ambient PM particles reach mouse brain due to permeability of the blood brain barrier, resulting in neuroinflammation, tangles and plaque formation similar to Alzheimer’s disease [4]. Carbon black particles have been detected in human placental tissue crossing the blood placental barrier [7], and magnetite has been detected in human brain [8], indicating that ultrafine PM particles can enter into different organ systems [9]. However, it is difficult to detect the amount of PM particles in different tissues because of the variable size and complex chemical nature. Consequently, there are few studies focused on detecting the amount of $PM_{2.5}$ in different tissues to determine the rates of deposition. Knowing the precise deposition process and the

transport mechanism of inhalable particles is crucial for health risk assessment and evaluation of target organ injury [10]. In this study, we used field emission scanning electron microscopy (FE-SEM) to visualize $PM_{2.5}$ particles, and fluorescence lifetime imaging microscopy (FLIM) to quantify $PM_{2.5}$ particles in lung and heart tissues. The deposition of $PM_{2.5}$ in different tissues has adverse effects on the target organs including tissue injury and inflammation [11] that are causally linked to cardiopulmonary diseases such as atherosclerosis, coronary heart disease and chronic obstructive pulmonary disease. Amyloids can accumulate not only in brain but also in different tissues and body organs that result in clinical syndromes [12]. A recent study has shown multiorgan amyloidosis in a coal miner [13]. A previous report has suggested that amyloid protein could be produced in tissues and might be derived from precursors in the blood circulation [14]. Studies have found increase in inflammatory cytokines in serum, heart, liver and lung of $PM_{2.5}$-exposed mice [15, 16, 17, 18], histological and immunohistochemical analysis would be the preferred method to directly observe the amyloid deposition and inflammation in tissues [19]. In this study, histological and immunohistochemical staining were used to evaluate inflammation and amyloid deposition in lung and heart. Moreover, chemical composition of $PM_{2.5}$ particles was also evaluated.

Results

Detection and quantification of $PM_{2.5}$ particles in lung and heart tissues by fluorescence lifetime imaging microscopy (FLIM)

Sixteen mice were divided equally into filtered air (FA) (control) (**Fig 1A**), and 2X concentrated air (**Fig 1B**) groups, and given the FA or concentrated $PM_{2.5}$ exposure. The mean concentrations of $PM_{2.5}$ in dirty air and FA chambers during the exposure were 71.20 ± 45.01 and 11.76 ± 4.40 μg/m^3, respectively. The mean outdoor $PM_{2.5}$ concentration during the exposure was 43.00 ± 6.05 μg/m^3. $PM_{2.5}$ particles from air pollution entered into lungs and were distributed to heart through blood circulation. **Fig 1C** presents a graphical illustration showing the movement of $PM_{2.5}$ particles inside the respiratory and blood circulation systems. FLIM microscopy enabled label-free detection and quantification of $PM_{2.5}$ particles on lung and heart tissues of mouse. Fluorescence spectra of $PM_{2.5}$ in PBS and tissues showed large overlap between 450 nm and 550 nm **(Fig 1D)**. Thus, it is hard to distinguish $PM_{2.5}$ from the tissues. However, the fluorescence lifetime of $PM_{2.5}$ and tissues were quite different, the lifetime of $PM_{2.5}$ was much shorter than that of tissues (**Fig. 1E**). Based on the different lifetime values, the green dots denote PM particles in tissues and the red fluorescence reveals the tissue structure. During respiration, the $PM_{2.5}$ particles enter directly into lungs and alveoli lined with blood capillaries. Lung tissues from the filtered air group showed little deposition of $PM_{2.5}$ particles (**Fig 1H**). Lung tissues from the dirty air group showed large numbers of $PM_{2.5}$ particles (**Fig. 1K**). The blood capillaries absorb oxygen and $PM_{2.5}$ particles from lung during respiration and transport to heart (**Fig 1N**). Heart absorbs and collects higher amounts of $PM_{2.5}$ particles from dirty air (**Fig 1Q**). The particle densities in lung and heart of mice were estimated (**Fig. 1R**) accordingly. The results showed that the median numbers of particles in lung of

$PM_{2.5}$-treated mice are 3.4 times more than that in the FA-treated mice, and that of in heart of $PM_{2.5}$-treated mice are 1.3 times more than that in FA-treated mice. The dispersion of data in lung tissues is relatively large.

Fig. 1 Mice were kept in exposure chambers for six months. Graphical illustrations (**A**) Mouse in filtered air chamber. (**B**) Mouse in dirty air chamber. (**C**) Movement of $PM_{2.5}$ particles into the respiratory track and accumulation in lungs and heart. (**D**) Fluorescence spectra of $PM_{2.5}$ in PBS and tissues. (**E**) Typical lifetime decay curves of $PM_{2.5}$ in tissues (green) and autofluorescence of tissues (red). (**F**) Auto-fluorescent image of lung tissue from filtered air. (**G**) $PM_{2.5}$ particles from filtered air. (**H**) Fluorescent deposition pattern of $PM_{2.5}$ particles in lung tissue from filtered air. (**I**) Auto-fluorescent image of lung tissue from dirty air. (**J**) $PM_{2.5}$ particles from dirty air. (**K**) Fluorescent deposition pattern of $PM_{2.5}$ particles in lung tissue from dirty air. (**L**) Auto-fluorescent image of heart tissue from filtered air. (**M**) Green dots are the $PM_{2.5}$ particles. (**N**) Fluorescent deposition pattern of $PM_{2.5}$ particles in heart tissue from filtered air. (**O**) Auto-fluorescent image of heart tissue from dirty air. (**P**) Green dots are the $PM_{2.5}$ particles. (**Q**) Fluorescent deposition pattern of $PM_{2.5}$ particles in heart tissue from dirty air. Scale bar: 20 μm. The resolution of FLIM images is 250 nm. (**R**) The estimated particle density in lung and heart of mice.

Exposure to concentrated $PM_{2.5}$ particles caused lung injury

Surface evaluation of tissues by field emission scanning electron microscopy (FE-SEM) showed that lung tissue sections from filtered air group showed no abnormality (**Fig. 2A**), whereas $PM_{2.5}$ particles (**Fig. 2B**), amyloid deposits (**Fig. 2C to 2F**), and damages (**Fig. 2G to 2H**) were detected in lung tissue sections from the dirty air exposure group. The effects of $PM_{2.5}$ particles on lung tissue sections were determined by histopathological evaluations. Hematoxylin and eosin (H&E) staining of lung tissue from filtered air (control) showed no abnormality (**Fig. 2I**), whereas lung tissue from dirty air exposure group showed damage (**Fig. 2J**). The lung tissues from filtered air (control) exposure group showed no abnormality (**Fig. 2K**), whereas lung tissue from dirty air exposure group showed inflammation (**Fig. 2L**). Congo red staining of lung tissues from filtered air showed no abnormality (**Fig. 2M**), whereas lung tissue from dirty air showed amyloid deposition (**Fig. 2N**). Moreover, immunohistochemistry with Aβ antibody found no abnormality in lung tissues from filtered air (**Fig. 2O**), whereas lung tissue from dirty air showed amyloid deposits (**Fig. 2P**). Immunohistochemistry with allograft inflammatory factor 1 (AIF1/IBA-1) antibody found no abnormality in lung tissues from filtered air (**Fig. 2Q**), whereas inflammation was detected in lung tissues from dirty air exposure group (**Fig. 2R**).

Fig. 2 Field emission scanning electron microscopy (FE-SEM) of lung tissues. (**A**) lung tissues from filtered air showed no abnormality, whereas (**B**) lung tissue from dirty air exposure group showed $PM_{2.5}$ particles, (**C** to **F**) amyloid deposits, and tissue damages (**G** to **H**). Histopathological evaluation by H&E staining showed morphology of air spaces in lung tissues. (**I**) lung tissue from filtered air (control) exposure group showed no abnormality, whereas (**J**) lung tissue from dirty air exposure group showed abnormality. Moreover, H&E staining showed morphology of bronchus in lung tissues, (**K**) lung tissue

from filtered air (control) exposure group showed no abnormality, whereas (**L**) lung tissue from dirty air exposure group showed inflammation. Congo red staining, (**M**) lung tissues from filtered air showed no abnormality, whereas (**N**) lung tissue from the dirty air showed amyloid deposition. Immunohistochemistry with Aβ antibody (1:500), (**O**) from lung of filtered air showed no abnormality, whereas (**P**) lung tissue from dirty air showed amyloid deposits. Immunohistochemistry with IBA-1 antibody (1:100), (**Q**) lung tissues from normal air showed no abnormality, whereas (**R**) lung tissue from dirty air showed inflammation. Magnification (**A**) 2k, scale bar: 20µm. Magnification (**B, C, E, G,** and **H**) 20k, Scale bar: 2µm. Magnification (**D** and **F**) 50k, Scale bar: 1µm.

Exposure to concentrated $PM_{2.5}$ particles caused heart tissue injury

Surface evaluation of tissues by FE-SEM showed that heart tissue sections from the filtered air group showed no abnormality (**Fig. 3A**), whereas $PM_{2.5}$ particles (**Fig. 3B** and **3C**), amyloid deposit (**Fig. 3D** and **3E**), and tissue damage (**Fig. 3F**) were detected in heart tissue sections from dirty air exposure group. Moreover, the effects of $PM_{2.5}$ particles on heart tissue sections were determined by histopathological evaluations. Congo red staining of heart tissues from filtered air showed no abnormality (**Fig. 3G**), whereas heart tissue from dirty air showed amyloid deposition (**Fig. 3H** and **3I**). Moreover, immunohistochemistry with Aβ antibody found no abnormality in heart tissues from filtered air (**Fig. 3J**), whereas heart tissue from dirty air showed amyloid deposits (**Fig. 3K** and **3L**). Immunohistochemistry with IBA-1 antibody found no abnormality in heart tissues from filtered air (**Fig. 3M**), whereas inflammation in heart tissues from the dirty air exposure group was detected (**Fig. 3N and 3O**).

Fig. 3 Filed emission scanning electron microscopy of heart tissues. (**A**) Heart tissues from filtered air showed no abnormality, whereas (**B** and **C**) heart tissue from dirty air exposure group showed $PM_{2.5}$ particles, (**D** and **E**) amyloid deposit, and (**F**) tissue damage. Histopathological evaluation by Congo red staining, (**G**) heart tissues from filtered air showed no abnormality, whereas (**H** and **I**) heart tissue from the dirty air showed amyloid deposition. Immunohistochemistry with Aβ antibody (1:500), (**J**) from heart of filtered air showed no abnormality, whereas (**K** and **L**) heart tissue from dirty air showed amyloid deposits. Immunohistochemistry with IBA-1 antibody (1:100), (**M**) heart tissues from filtered air showed no abnormality, whereas (**N** and **O**) heart tissue from dirty air showed inflammation. Magnification (**A, B** and **E**) 20k, scale bar: 2 µm. Magnification (**C**) 50k, scale bar 1 µm. Magnification (**D**) 10k, scale bar: 5 µm. Magnification (**F**) 100k, scale bar 500nm. Magnification (**G** to **O**) 40X, Scale bar: 500 µm.

The organic components of $PM_{2.5}$ in dirty air and FA chambers

The element composition in dirty air and FA were detected by mass spectrometry. The **Figures 4A** and **4B** showed the mass spectra of samples and the ratios of different element compositions in FA and dirty air groups. The numbers of elements combination in dirty air and FA are shown in **Tables 1** and **2**. The results indicated that dirty air group showed more organic substances, characterized by CHON, CHNaO, CHNNa, CHONS, CHNNaO, CHO, CHOS and CHONS when compared with FA group.

Table 1 The organic element combination in air samples at positive and negative modes (ESI+ and ESI-) in (**A**) filtered air (FA), and (**B**) dirty air. An Agilent 1200 series HPLC with a C18 column (SB-C18, 3.0 × 100 mm, 1.8 μm) was used for chromatographic separation. At ESI+, a: $C_6H_{11}NO$; b: $C_6H_{13}NO_2$; c: $C_{16}H_{22}O_4$; d: $C_{22}H_{43}NO$; e: $C_{22}H_{42}O_4$; At ESI-, A: $C_3H_6O_3$; B: $C_{16}H_{32}O_2$; C: $C_{18}H_{36}O_2$; D: $C_{20}H_{40}O_6$; E: $C_{22}H_{44}O_6$; F: $C_{24}H_{44}N_4O_4$; G: $C_{30}H_{55}N_5O_5$; H: $C_{35}H_{70}N_2O_{10}$

Table 1 The mass spec elemental analysis in FA and dirty air at ESI+

Element Combination	Numbers in FA	Numbers in Dirty air (PM)
CHO	83	104
CHN	11	16
CHOS	2	3
CHNS	1	1
CHON	136	236
CHNaO	14	21
CHNNa	1	1
CHONS	3	8
CHNNaO	35	34
CHONaS	1	0
CHNNaS	1	0
CHONSNa	1	1
Total	289	426

Table 2 The elemental analysis in FA and dirty air at ESI-

Element Combination	Numbers in FA	Numbers in dirty air (PM)
CHO	89	139
CHS	0	2
CHN	0	0
CHOS	26	29
CHNS	2	2
CHON	71	84
CHONS	9	9
Total	197	265

The metal components of $PM_{2.5}$ in dirty air and FA chambers

The samples of $PM_{2.5}$ in dirty air and FA chambers were collected weekly during the exposure. Because of the hazards of heavy metals in air borne particulate matter, we measured 8 heavy metals including Zn, Bi, Cd, Ni, Fe, Mn, Cr and Cu by ICP-MS in this study. **Fig. S1** shows the fractograms of the 8 metals. As shown in **Table S1**, the concentrations of these 8 elemental components in dirty air were about five times more than those in the FA chamber, demonstrating that the METAS we used to give the mice dirty air and FA exposure significantly concentrated the ambient $PM_{2.5}$ without changing its components. Of these 8 metals, Fe, Zn, Cd and Mn are the main components.

Discussion

Numerous studies have indicated the association between air borne particulate matter and diseases in humans and experimental animals. This includes cardiopulmonary diseases, diabetes, cerebrovascular diseases and reproductive toxicity [20, 21]. As the main air pollutant, the association between fine particulate matter ($PM_{2.5}$) and health is of great concern. This is particularly problematic in heavily industrialized and populated areas, with China often identified as a region with the highest $PM_{2.5}$ concentration in the world [22]. In 2020, the annual average concentration of $PM_{2.5}$ in China was 36 $\mu g/m^3$, lower than that in 2017 (43 $\mu g/m^3$), but still higher than both Chinese air quality standard (35 $\mu g/m^3$) and U.S EPA standard (12 $\mu g/m^3$) [22]. In this study, the mice were exposed to concentrated $PM_{2.5}$ using METAS [23]. The concentrations in dirty air and FA chambers were 71.20 $\mu g/m^3$ and 11.76 $\mu g/m^3$, respectively. Airborne PM particles enter into lung tissue by passive transport along surface liquids, and phagocytosis within alveolar macrophages [24]. Although several lines of evidence support the theory that particles translocate from lung into the circulation, then enter into heart, liver and kidney, quantifying the particles in these organs took precedence in assessing particle toxicological effects. Previous studies

have used second harmonic generation (SHG) to detect black carbon in placenta [7] and high-resolution transmission electron microscopy (HRTEM) to detect magnetite in brain [8], but there are few studies to quantify the amounts of $PM_{2.5}$ in tissues. It is noteworthy that airborne $PM_{2.5}$ was a mixture but not a single chemical, which made the detection more difficult. In this study, FLIM enabled label free detection and quantification of PM particles with high resolution on lung and heart tissues, which can provide broad insights into the distribution of particles entering into tissues. Compared with transmission electron microscopy (TEM), FLIM has several advantages: sample preparation is simple and does not need special treatment; the imaging range of FLIM is larger than TEM, which is convenient for large samples statistics. In this study PM particles were also detected in the filtered air group because filters do not have 100 percent efficiency, and extremely small particles can pass through them. Our current study found that the amounts of $PM_{2.5}$ was higher in dirty air (PM) group than that in FA group. Intriguingly, $PM_{2.5}$ was more in heart than lung, probably because lung has air sacs and the PM particles are cleared by transportation over fluid and phagocytosis [24], whereas heart is the muscular organ that pumps oxygenated blood along with dissolved PM particles of various sizes and chemical compositions from lungs. The powerful mechanical force of blood passing through different chambers of the heart may contribute to adsorption of $PM_{2.5}$ particles into heart muscles, which act as a sink for inhaled particulate matter.

Inhalation of $PM_{2.5}$ particles have adverse health effects. Exposure to $PM_{2.5}$ over shorter periods of time reduced lung function in children [25]. The results showed that exposure to dirty air containing $PM_{2.5}$ particles damaged lung tissues (**Fig. 2**). Previous studies have shown that $PM_{2.5}$ exposure was associated with the release of inflammatory cytokines and inflammatory cell infiltration. A recent study has shown that activation of the NLRP3/ caspase-1 signaling pathway by $PM_{2.5}$ particles induced pulmonary inflammation [26]. The mechanism of inflammation in pulmonary diseases has been reviewed recently [27]. Inflammatory response has been certified as a vital mechanism linking particulate matter and adverse effects, and our results directly verified the occurrence of inflammation. Chronic inflammation and amyloidosis directly target lungs, severely effect alveolar structures, hamper gaseous exchange and result in serious respiratory impairment including asthma and other pulmonary diseases [27]. In this study we have found amyloid deposition in lung tissues (**Fig. 2C to 2F, Fig. 2N and 2P**), that suggests tissue stiffness and fluid buildup that lead to the dilation of air spaces and systemic inflammation (**Fig. 2G to 2H**). Pulmonary inflammation is a risk factor for cardiovascular diseases [28]. In this study heart tissues from dirty air exposure group containing $PM_{2.5}$ particles showed amyloid deposits (**Fig. 3D, 3E, 3H, 3I, and 3L**) and inflammation (**Fig. 3N and 3O**). Inflammation is common in coronary heart diseases and atherosclerosis but the mechanism is not known. Moreover, amyloids can infiltrate heart tissues and result in cardiac amyloidosis. Cardiac amyloidosis results in myocardial thickening and dysfunction [29]. The results from the current study suggests that air pollution is one of the causative factors for rising levels of chronic pulmonary and cardiac diseases [30, 31] and that particulate induced amyloidosis is a potential mechanism for targeted therapeutic development.

A previous human study found metal components (e.g. Al, Fe, Ca, Ni, Cu, Pb, V and Zn) of $PM_{2.5}$ significantly decreased whole blood coagulation time in healthy subjects [32]. $PM_{2.5}$ rich in metal components such as nickel (Ni) has been linked to adverse cardiopulmonary effects [33, 34]. Moreover, other studies also found that metal constituents such as Zn, Cd, Mn, Cu [35], Cd, Pb [36] in $PM_{2.5}$ were associated with a variety of adverse health effects. In this study, we determined eight main (Zn, Bi, Cd, Ni, Fe, Mn, Cr and Cu) metals in $PM_{2.5}$, in which the concentration of Fe, Zn, Cd and Mn are higher than other metals. The organic components in dirty air and FA were also evaluated in this study. Sulfur and nitrogen containing organics have received the most attention because they can be used to reveal the pollutant sources, and aging mechanisms. CHON species that can form via gas-phase nitrate radical initiated oxidation are also significant components of secondary organic aerosol [37]. A previous study indicated that CHN species were a significant contributor to the organic matter at the Beijing site, and high levels of CHN species and their CH2 homologous series were identified as quinoline and benzo [f] quinoline compounds, which may have considerable health implications [38]. Therefore, chemical characteristics of organic aerosols can provide a clue for exploring the adverse effects of ambient particulate matter. Moreover, the components of air pollution are associated to increased hospital visits for pulmonary and cardiac ailments [39].

Conclusion

In this study fluorescence lifetime imaging microscopy enabled label-free detection and quantification of $PM_{2.5}$ particles on lung and heart tissues of mouse. The work presented solid evidence and insights on toxicological effects of $PM_{2.5}$ exposure to chronic lung and heart injuries. It suggested rising levels of air pollution are linked to increased cardiopulmonary diseases worldwide.

Materials And Methods

Animal management

Six weeks old *Mus musculus* (C57BL/6 male mice) were purchased from Shanghai Jiesijie Laboratory Animal Co., Ltd (Shanghai, China). They were housed in a pathogen-free animal facility at Fudan University, at constant temperature (21°C ± 1°C) and humidity (60%) on a day and night cycle of 12 hours each, and were maintained on normal chow diet. The procedures were approved by the Institutional Research Committees of the Fudan University, Shanghai, China, and the methods were performed in accordance with the set regulations and guidelines.

Exposure of concentrated $PM_{2.5}$ particles to mice

Sixteen mice were divided into two groups and were exposed to concentrated $PM_{2.5}$ (PM, dirty air), and filtered air (FA, control), using the “Shanghai Meteorological and Environmental Animal Exposure System (Shanghai-METAS)”, located in the School of Public Health at Fudan University at Xujiahui District in

Shanghai. We have used the exposure system to perform several studies [23, 40]. The machine filtered the larger particles, and only the particles with diameters less than 2.5μm entered into the chamber.

In this study, the exposure lasted for 8 h per day, 6 days per week, in a total of 24 weeks. The mice were freely allowed to eat food and drink water.

The real-time concentration of $PM_{2.5}$ particles

The real-time concentrations of $PM_{2.5}$ from exposure chamber and control chamber were continuously measured by TEOM (Thermo Fisher Scientific, Waltham, MA), and $PM_{2.5}$ were sampled on Teflon filters (Gelman Teflon, 37 mm, 0.2 mm pore) for subsequent measuring the accurate concentrations and the components such as constituents of polycyclic aromatic hydrocarbons (PAHs) and trace metals.

Metal concentration and component analysis of $PM_{2.5}$ particles

The Teflon filter (Gelman Teflon, 37 mm, 0.2 mm pore) with $PM_{2.5}$ was cut and divided into two parts. The filters were treated with 10 mL of 60% high-purity nitric acid (HNO_3) and 3 mL of 37% perchloric acid ($HClO_4$). The solutions containing filters were heated in microwave for 1 h. They were then stored at 4°C until analysis. The metal concentrations of $PM_{2.5}$ particles were determined using an Inductive Coupled Plasma Emission Spectrometer (Atom Scan 2000, Jarrell-Ash, USA).

Organic component analysis of $PM_{2.5}$ in dirty air and FA

The filters with $PM_{2.5}$ were cut into pieces using scissors and extracted in 30 mL methanol under ultrasonication for 30 min. The extracted solution was filtered (polytetrafluoroethylene membrane) through a syringe with 0.2 μm pore size. After concentration, the final volume was roughly 1 ml prior to HPLC-DAD-Q-TOF-MS analysis. An Agilent 1200 series HPLC with a C18 column (SB-C18, 3.0 × 100 mm, 1.8 μm) was used for chromatographic separation with an injection volume of 2 μL. The flow rate was set to 0.4 mL/min and the gradient separation was conducted with 0.1% formic acid in water (A) and methanol (B). The concentration of B was 5% for the first 0.5 min increased to 95% from 0.5 to 27 min, and then decreased back to 5% from 27 to 27.1 min. The identification of BrC was determined with an Agilent 6520 Q-TOF-MS and an Agilent G1315D diode array detector (DAD). UV-Vis absorption was measured using the DAD detector over the wavelength range of 190–600 nm. The TOF-MS was equipped with electrospray ionization (ESI), operated in both positive and negative ion modes. The drying gas flow rate was 7 L/min, and the temperature and flow rate of sheath gas were 350°C and 11 L/min, respectively.

Preparation of heart and lung tissue sections

The protocol approved by the institutional review board was followed, the mice were sacrificed, and heart and lung samples were collected and immediately stored at -80°C until sectioning. The samples were attached to the aluminum disc and 10-μm-thick tissue slices were prepared using Leica CM1950 cryostat

(Leica Biosystems), attached over the surface of adhesion microscopic glass slides, and stored in airtight falcon tubes at -80°C before analyses.

Field emission scanning electron microscopy (FE-SEM)

The falcon tubes containing glass slides of heart or lung cryo-sections were dried at room temperature before analysis without any pretreatment. The surface of the FE-SEM aluminum sample stage was covered with carbon conducting tape and the glass slide was attached onto it. A Hitachi S-4800 field emission scanning electron microscope (FE-SEM) equipped with Bruker Xflash 6160 detector was used for observation of heart or lung tissue sections of eight mice from dirty air and eight mice from filtered air, at acceleration voltage of 1.0 kV, and emission current of 10 μA. The vacuum level in the observation chamber was ~ 10^{-7} Pa. The observations were made at the working distance of 2.1 mm to 2.4 mm, and at the scan speed of 20 seconds for each figure, at 10k, 20k, 50k, and 100k magnifications.

Fluorescence lifetime imaging microscopy (FLIM)

The fluorescence spectra of $PM_{2.5}$ particles in PBS solution and the tissues were excited by a 405 nm CW laser (BDL-405-SMC, Becker and Hickl, Berlin, Germany) and recorded by an optical fiber spectrometer (Ocean Optics, USB2000+, Dunedin, FA, USA) with a 420 nm long-pass filter. The $PM_{2.5}$ particles in frozen tissues were imaged using a laser scanning microscope (FV300/IX71, Olympus, Japan) equipped with a femtosecond (fs) pulsed laser (680–1300 nm tunable wavelength, 150 fs, 80MHz, InSight X3 Dual, USA) and a time correlated single photon counting (TCSPC) system (SPC-150, Becker & Hickl, Germany), with a 60× water-dipping objective (NA = 1.2). The fluorescence lifetime imaging microscopy (FLIM) were excited by the 830 nm fs laser collected by a 770 nm (longpass) LP. The $PM_{2.5}$ particles in PBS solution were measured by FLIM as well to obtain the fluorescence lifetime of $PM_{2.5}$. Each figure had a field of 123 m × 123 m with 256 × 256 pixels, collecting the signal within the depth of about 2 μm. At least 6 different areas were randomly imaged for each sample. The mean lifetime of each pixel is fitted with multi-exponential decay models and calculated using the commercial SPCImage software package (Becker & Hickl GmbH, Berlin, Germany). The fluorescence lifetime of $PM_{2.5}$ solution was mostly in the range of 170–200 ps with the peak at 174 ps. Therefore, the FLIM images of tissues with $PM_{2.5}$ were fitted by setting the shortest fluorescence lifetime component as 174 ps. Then the pixels with short lifetime were marked as green noting $PM_{2.5}$ particles, and the pixels with long lifetime were depicted as red denoting tissue autofluorescence. $PM_{2.5}$ particle density in the lung or heart tissues of $PM_{2.5}$- or FA-treated mice were calculated based on the two-colored images.

Histological and immunohistochemical staining

The heart and lung tissues were subjected to Congo red staining for histological and morphological information. Congo red dye was obtained from Ruibao and Biotech Co., Ltd (Cat # R1029). For immunohistochemical analyses the following antibodies and materials were used: IBA-1 (Reego and Biology, 1:100), Aβ (Reego and Biology, 1:500). HRP-labelled goat anti-rabbit secondary antibody (Reego and Biology, 1:200), DAB (DAKO, K5007), normal rabbit serum (Boster, AR1010), and BSA (Solarbio,

A8020). High resolution optical images of the stained tissues were observed by Olympus CKX53 microscope and recorded by using Olympus cellSens 2.1 [ver.2.1] imaging software for Life Sciences (Olympus, Tokyo, Japan).

Declarations

Ethics approval and consent to participate

The animal study procedures were approved by the Institutional Research Committees of the Fudan University, Shanghai, China, and the methods were performed in accordance with the set regulations and guidelines.

Consent for publication

Not applicable

Availability of data and materials

All data generated or analysed during this study are included in this published article [and its supplementary information files].

Competing interests

The authors declare no competing interests.

Fundings

SH thank the Kempe Foundation Sweden, and to Scientific Research Startup Foundation (IDH1615113) of Fudan University to RNZ. JZ thanks the National Natural Science Foundation of China (91543119, 81673125) for funding.

Authors' contributions

Study design: SH/JZ. Data collection: SH/KP/WS/LM/JZ. Data analysis and interpretation: SH/MT/LM/JZ. Manuscript draft: SH/MT/JZ. Critical revision and final decision to submit: all authors. The author(s) read and approved the final manuscript

Acknowledgments

We are grateful to Prof. Richard N. Zare of Department of Chemistry, Stanford University for guidance and support. We are thankful to Malin Linder Nording, Department of Chemistry, Umea University, Sweden for valuable assistance in drafting the manuscript.

References

1. Woodward NC, Crow AL, Zhang Y, Epstein S, Hartiala J, Johnson R, et al. Exposure to Nanoscale Particulate Matter from Gestation to Adulthood Impairs Metabolic Homeostasis in Mice. Sci Rep. 2019;9 1:1816; doi: 10.1038/s41598-018-37704-2.
2. Al-Kindi SG, Brook RD, Biswal S, Rajagopalan S. Environmental determinants of cardiovascular disease: lessons learned from air pollution. Nat Rev Cardiol. 2020;17 10:656–72; doi: 10.1038/s41569-020-0371-2.
3. Li D, Li Y, Li G, Zhang Y, Li J, Chen H. Fluorescent reconstitution on deposition of PM(2.5) in lung and extrapulmonary organs. Proceedings of the National Academy of Sciences of the United States of America. 2019;116 7:2488-93; doi: 10.1073/pnas.1818134116. https://pubmed.ncbi.nlm.nih.gov/30692265, https://www.ncbi.nlm.nih.gov/pmc/articles/PMC6377456/.
4. Hameed S, Zhao J, Zare RN. Ambient PM particles reach mouse brain, generate ultrastructural hallmarks of neuroinflammation, and stimulate amyloid deposition, tangles, and plaque formation. Talanta Open. 2020;2:100013; doi: https://doi.org/10.1016/j.talo.2020.100013. https://www.sciencedirect.com/science/article/pii/S2666831920300138.
5. Pankhurst Q, Hautot D, Khan N, Dobson J. Increased levels of magnetic iron compounds in Alzheimer's disease. Journal of Alzheimer's disease: JAD. 2008;13 1:49–52; doi: 10.3233/jad-2008-13105. http://www.ncbi.nlm.nih.gov/pubmed/18334756.
6. Hautot D, Pankhurst QA, Khan N, Dobson J. Preliminary evaluation of nanoscale biogenic magnetite in Alzheimer's disease brain tissue. Proceedings Biological sciences. 2003;270 Suppl 1:S62-4; doi: 10.1098/rsbl.2003.0012. http://www.ncbi.nlm.nih.gov/pubmed/12952638.
7. Bové H, Bongaerts E, Slenders E, Bijnens EM, Saenen ND, Gyselaers W, et al. Ambient black carbon particles reach the fetal side of human placenta. Nat Commun. 2019;10 1:3866; doi: 10.1038/s41467-019-11654-3.
8. Maher BA, Ahmed IA, Karloukovski V, MacLaren DA, Foulds PG, Allsop D, et al. Magnetite pollution nanoparticles in the human brain. Proceedings of the National Academy of Sciences of the United States of America. 2016;113 39:10797–801; doi: 10.1073/pnas.1605941113. http://www.ncbi.nlm.nih.gov/pubmed/27601646.
9. Kreyling WG, Hirn S, Möller W, Schleh C, Wenk A, Celik G, et al. Air-blood barrier translocation of tracheally instilled gold nanoparticles inversely depends on particle size. ACS Nano. 2014;8 1:222–33; doi: 10.1021/nn403256v.
10. Patton JS, Byron PR. Inhaling medicines: delivering drugs to the body through the lungs. Nat Rev Drug Discov. 2007;6 1:67–74; doi: 10.1038/nrd2153.
11. Pietropaoli AP, Frampton MW, Hyde RW, Morrow PE, Oberdörster G, Cox C, et al. Pulmonary function, diffusing capacity, and inflammation in healthy and asthmatic subjects exposed to ultrafine particles. Inhal Toxicol. 2004;16 Suppl 1:59–72; doi: 10.1080/08958370490443079.
12. Bustamante JG ZS. Amyloidosis. Treasure Island (FL): StatPearls Publishing, 2022.

13. Gołębiowski T, Kuźniar J, Porażko T, Wojtala R, Konieczny A, Krajewska M, et al. Multisystem Amyloidosis in a Coal Miner with Silicosis: Is Exposure to Silica Dust a Cause of Amyloid Deposition? Int J Environ Res Public Health. 2022;19 4:2297; doi: 10.3390/ijerph19042297. https://pubmed.ncbi.nlm.nih.gov/35206498, https://www.ncbi.nlm.nih.gov/pmc/articles/PMC8871531/.
14. Joachim CL, Mori H, Selkoe DJ. Amyloid β-protein deposition in tissues other than brain in Alzheimer's disease. Nature. 1989;341 6239:226–30; doi: 10.1038/341226a0. https://doi.org/10.1038/341226a0.
15. Cong LH, Li T, Wang H, Wu YN, Wang SP, Zhao YY, et al. IL-17A-producing T cells exacerbate fine particulate matter-induced lung inflammation and fibrosis by inhibiting PI3K/Akt/mTOR-mediated autophagy. J Cell Mol Med. 2020;24 15:8532–44; doi: 10.1111/jcmm.15475.
16. Ge C, Tan J, Zhong S, Lai L, Chen G, Zhao J, et al. Nrf2 mitigates prolonged PM2.5 exposure-triggered liver inflammation by positively regulating SIKE activity: Protection by Juglanin. Redox Biol. 2020;36:101645; doi: 10.1016/j.redox.2020.101645.
17. Yue W, Tong L, Liu X, Weng X, Chen X, Wang D, et al. Short term Pm2.5 exposure caused a robust lung inflammation, vascular remodeling, and exacerbated transition from left ventricular failure to right ventricular hypertrophy. Redox Biol. 2019;22:101161; doi: 10.1016/j.redox.2019.101161.
18. Zhang S, Zhang W, Zeng X, Zhao W, Wang Z, Dong X, et al. Inhibition of Rac1 activity alleviates PM2.5-induced pulmonary inflammation via the AKT signaling pathway. Toxicol Lett. 2019;310:61–9; doi: 10.1016/j.toxlet.2019.04.017.
19. Rajamohamedsait HB, Sigurdsson EM. Histological staining of amyloid and pre-amyloid peptides and proteins in mouse tissue. Methods Mol Biol. 2012;849:411–24; doi: 10.1007/978-1-61779-551-0_28. https://pubmed.ncbi.nlm.nih.gov/22528106, https://www.ncbi.nlm.nih.gov/pmc/articles/PMC3859432/.
20. Almetwally AA, Bin-Jumah M, Allam AA. Ambient air pollution and its influence on human health and welfare: an overview. Environ Sci Pollut Res Int. 2020;27 20:24815–30; doi: 10.1007/s11356-020-09042-2.
21. Schraufnagel DE, Balmes JR, Cowl CT, De Matteis S, Jung SH, Mortimer K, et al. Air Pollution and Noncommunicable Diseases: A Review by the Forum of International Respiratory Societies' Environmental Committee, Part 1: The Damaging Effects of Air Pollution. Chest. 2019;155 2:409–16; doi: 10.1016/j.chest.2018.10.042.
22. Du X, Chen R, Meng X, Liu C, Niu Y, Wang W, et al. The establishment of National Air Quality Health Index in China. Environ Int. 2020;138:105594; doi: 10.1016/j.envint.2020.105594.
23. Du XH, Jiang S, Zeng XJ, Zhang J, Pan K, Zhou J, et al. Air pollution is associated with the development of atherosclerosis via the cooperation of CD36 and NLRP3 inflammasome in ApoE(-/-) mice. Toxicol Lett. 2018;290:123 – 32; doi: 10.1016/j.toxlet.2018.03.022. <Go to ISI>://WOS:000430360500015.

24. Lippmann M, Yeates DB, Albert RE. Deposition, retention, and clearance of inhaled particles. Br J Ind Med. 1980;37 4:337–62; doi: 10.1136/oem.37.4.337.
25. Xu D, Chen Y, Wu L, He S, Xu P, Zhang Y, et al. Acute effects of ambient PM(2.5) on lung function among schoolchildren. Sci Rep. 2020;10 1:4061; doi: 10.1038/s41598-020-61003-4.
26. Jia H, Liu Y, Guo D, He W, Zhao L, Xia S. PM2.5-induced pulmonary inflammation via activating of the NLRP3/caspase-1 signaling pathway. Environ Toxicol. 2021;36 3:298–307; doi: 10.1002/tox.23035. https://pubmed.ncbi.nlm.nih.gov/32996690, https://www.ncbi.nlm.nih.gov/pmc/articles/PMC7891361/.
27. Aghasafari P, George U, Pidaparti R. A review of inflammatory mechanism in airway diseases. Inflamm Res. 2019;68 1:59–74; doi: 10.1007/s00011-018-1191-2.
28. Van Eeden S, Leipsic J, Paul Man SF, Sin DD. The relationship between lung inflammation and cardiovascular disease. Am J Respir Crit Care Med. 2012;186 1:11–6; doi: 10.1164/rccm.201203-0455PP.
29. McVeigh T, Tennyson C. Understanding and recognizing cardiac amyloidosis. Jaapa. 2020;33 10:16–20; doi: 10.1097/01.JAA.0000697236.11386.3a.
30. Amsalu E, Wang T, Li H, Liu Y, Wang A, Liu X, et al. Acute effects of fine particulate matter (PM2.5) on hospital admissions for cardiovascular disease in Beijing, China: a time-series study. Environmental Health. 2019;18 1:70; doi: 10.1186/s12940-019-0506-2. https://doi.org/10.1186/s12940-019-0506-2.
31. Hayes RB, Lim C, Zhang Y, Cromar K, Shao Y, Reynolds HR, et al. PM2.5 air pollution and cause-specific cardiovascular disease mortality. Int J Epidemiol. 2020;49 1:25–35; doi: 10.1093/ije/dyz114.
32. Sangani RG, Soukup JM, Ghio AJ. Metals in air pollution particles decrease whole-blood coagulation time. Inhalation toxicology. 2010;22 8:621–6; doi: 10.3109/08958371003599037. http://www.ncbi.nlm.nih.gov/pubmed/20388004.
33. Campen MJ, Nolan JP, Schladweiler MC, Kodavanti UP, Evansky PA, Costa DL, et al. Cardiovascular and thermoregulatory effects of inhaled PM-associated transition metals: a potential interaction between nickel and vanadium sulfate. Toxicological sciences: an official journal of the Society of Toxicology. 2001;64 2:243–52; doi: 10.1093/toxsci/64.2.243. http://www.ncbi.nlm.nih.gov/pubmed/11719707.
34. Graff DW, Cascio WE, Brackhan JA, Devlin RB. Metal particulate matter components affect gene expression and beat frequency of neonatal rat ventricular myocytes. Environmental health perspectives. 2004;112 7:792–8; doi: 10.1289/ehp.112-1241994. http://www.ncbi.nlm.nih.gov/pubmed/15159208.
35. Kogianni E, Kouras A, Samara C. Indoor concentrations of PM2.5 and associated water-soluble and labile heavy metal fractions in workplaces: implications for inhalation health risk assessment. Environmental science and pollution research international. 2020; doi: 10.1007/s11356-019-07584-8. http://www.ncbi.nlm.nih.gov/pubmed/31927729.
36. Xu P, He X, He S, Luo J, Chen Q, Wang Z, et al. Personal exposure to PM2.5-bound heavy metals associated with cardiopulmonary function in general population. Environmental science and

pollution research international. 2021;28 6:6691–9; doi: 10.1007/s11356-020-11034-1. http://www.ncbi.nlm.nih.gov/pubmed/33009612.

37. Faxon C, Hammes J, Le Breton M, Pathak RK, Hallquist M. Characterization of organic nitrate constituents of secondary organic aerosol (SOA) from nitrate-radical-initiated oxidation of limonene using high-resolution chemical ionization mass spectrometry. Atmos Chem Phys. 2018;18 8:5467-81; doi: 10.5194/acp-18-5467-2018. <Go to ISI>://WOS:000430492800006.
38. Jang KS, Choi M, Park M, Park MH, Kim YH, Seo J, et al. Assessment of PM2.5-bound nitrogen-containing organic compounds (NOCs) during winter at urban sites in China and Korea. Environmental pollution. 2020;265 Pt B:114870; doi: 10.1016/j.envpol.2020.114870. http://www.ncbi.nlm.nih.gov/pubmed/32504978.
39. Sarnat SE, Winquist A, Schauer JJ, Turner JR, Sarnat JA. Fine particulate matter components and emergency department visits for cardiovascular and respiratory diseases in the St. Louis, Missouri-Illinois, metropolitan area. Environ Health Perspect. 2015;123 5:437–44; doi: 10.1289/ehp.1307776.
40. Du X, Jiang S, Zeng X, Zhang J, Pan K, Song L, et al. Fine particulate matter-induced cardiovascular injury is associated with NLRP3 inflammasome activation in Apo E(-/-) mice. Ecotoxicol Environ Saf. 2019;174:92–9; doi: 10.1016/j.ecoenv.2019.02.064.

Figures

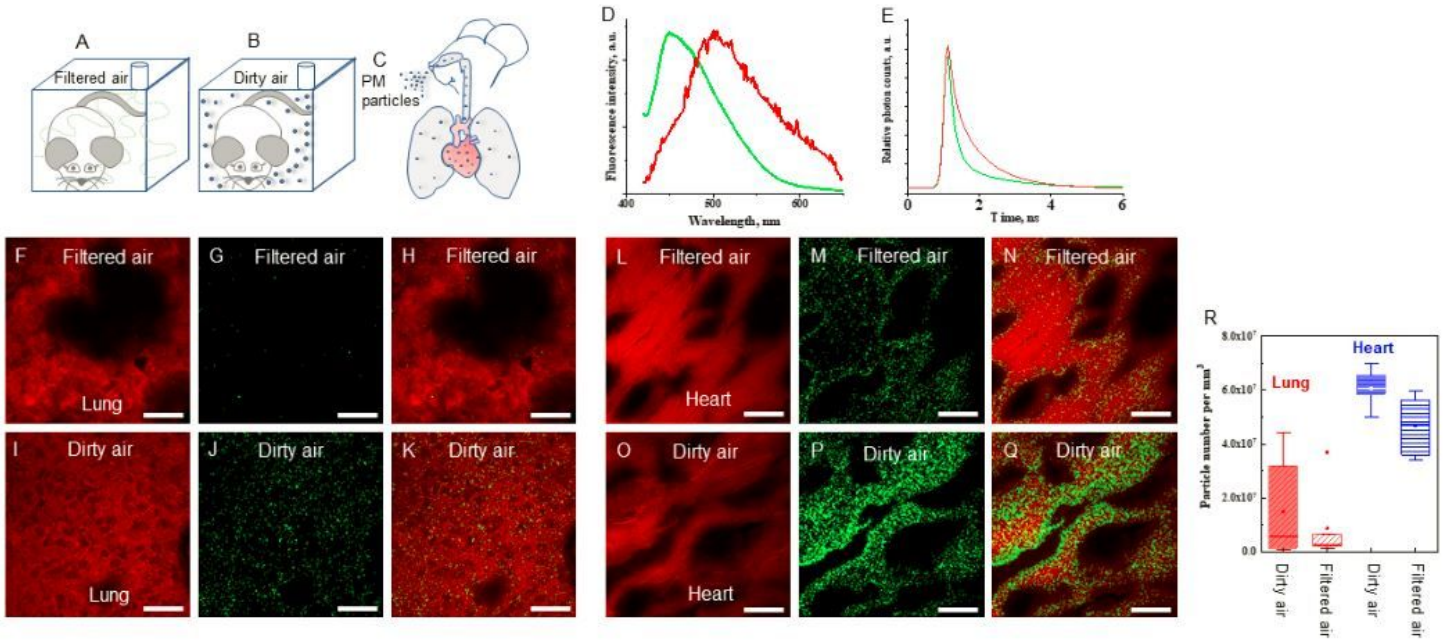

Figure 1

Mice were kept in exposure chambers for six months. Graphical illustrations (**A**) Mouse in filtered air chamber. (**B**) Mouse in dirty air chamber. (**C**) Movement of $PM_{2.5}$ particles into the respiratory track and

accumulation in lungs and heart. (**D**) Fluorescence spectra of $PM_{2.5}$ in PBS and tissues. (**E**) Typical lifetime decay curves of $PM_{2.5}$ in tissues (green) and autofluorescence of tissues (red). (**F**) Auto-fluorescent image of lung tissue from filtered air. (**G**) $PM_{2.5}$ particles from filtered air. (**H**) Fluorescent deposition pattern of $PM_{2.5}$ particles in lung tissue from filtered air. (**I**) Auto-fluorescent image of lung tissue from dirty air. (**J**) $PM_{2.5}$ particles from dirty air. (**K**) Fluorescent deposition pattern of $PM_{2.5}$ particles in lung tissue from dirty air. (**L**) Auto-fluorescent image of heart tissue from filtered air. (**M**) Green dots are the $PM_{2.5}$ particles. (**N**) Fluorescent deposition pattern of $PM_{2.5}$ particles in heart tissue from filtered air. (**O**) Auto-fluorescent image of heart tissue from dirty air. (**P**) Green dots are the $PM_{2.5}$ particles. (**Q**) Fluorescent deposition pattern of $PM_{2.5}$ particles in heart tissue from dirty air. Scale bar: 20 μm. The resolution of FLIM images is 250 nm. (**R**) The estimated particle density in lung and heart of mice.

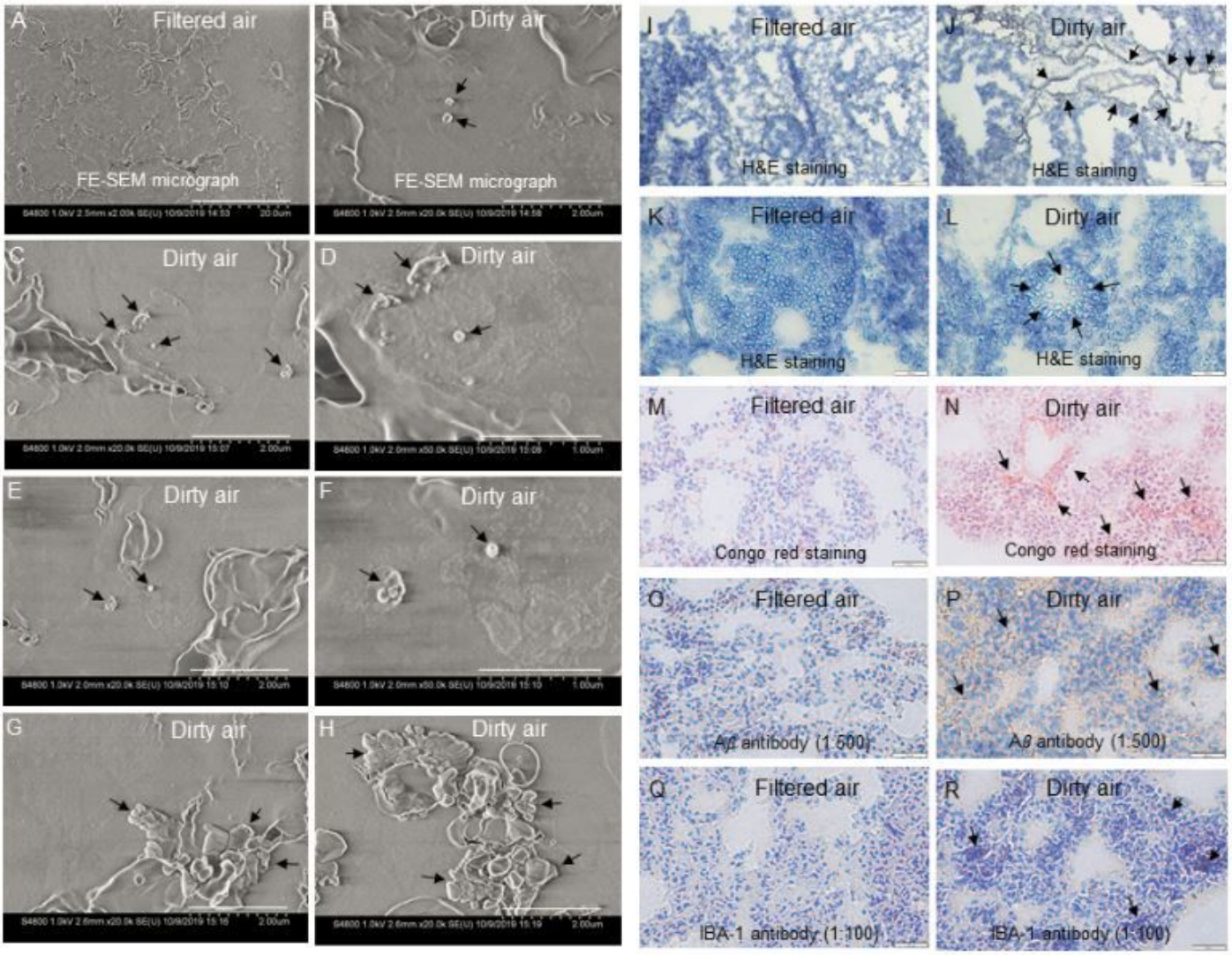

Figure 2

Field emission scanning electron microscopy (FE-SEM) of lung tissues. (**A**) lung tissues from filtered air showed no abnormality, whereas (**B**) lung tissue from dirty air exposure group showed $PM_{2.5}$ particles, (**C**

to **F**) amyloid deposits, and tissue damages (**G** to **H**). Histopathological evaluation by H&E staining showed morphology of air spaces in lung tissues. (**I**) lung tissue from filtered air (control) exposure group showed no abnormality, whereas (**J**) lung tissue from dirty air exposure group showed abnormality. Moreover, H&E staining showed morphology of bronchus in lung tissues, (**K**) lung tissue from filtered air (control) exposure group showed no abnormality, whereas (**L**) lung tissue from dirty air exposure group showed inflammation. Congo red staining, (**M**) lung tissues from filtered air showed no abnormality, whereas (**N**) lung tissue from the dirty air showed amyloid deposition. Immunohistochemistry with Aβ antibody (1:500), (**O**) from lung of filtered air showed no abnormality, whereas (**P**) lung tissue from dirty air showed amyloid deposits. Immunohistochemistry with IBA-1 antibody (1:100), (**Q**) lung tissues from normal air showed no abnormality, whereas (**R**) lung tissue from dirty air showed inflammation. Magnification (**A**) 2k, scale bar: 20µm. Magnification (**B, C, E, G,** and **H**) 20k, Scale bar: 2µm. Magnification (**D** and **F**) 50k, Scale bar: 1µm.

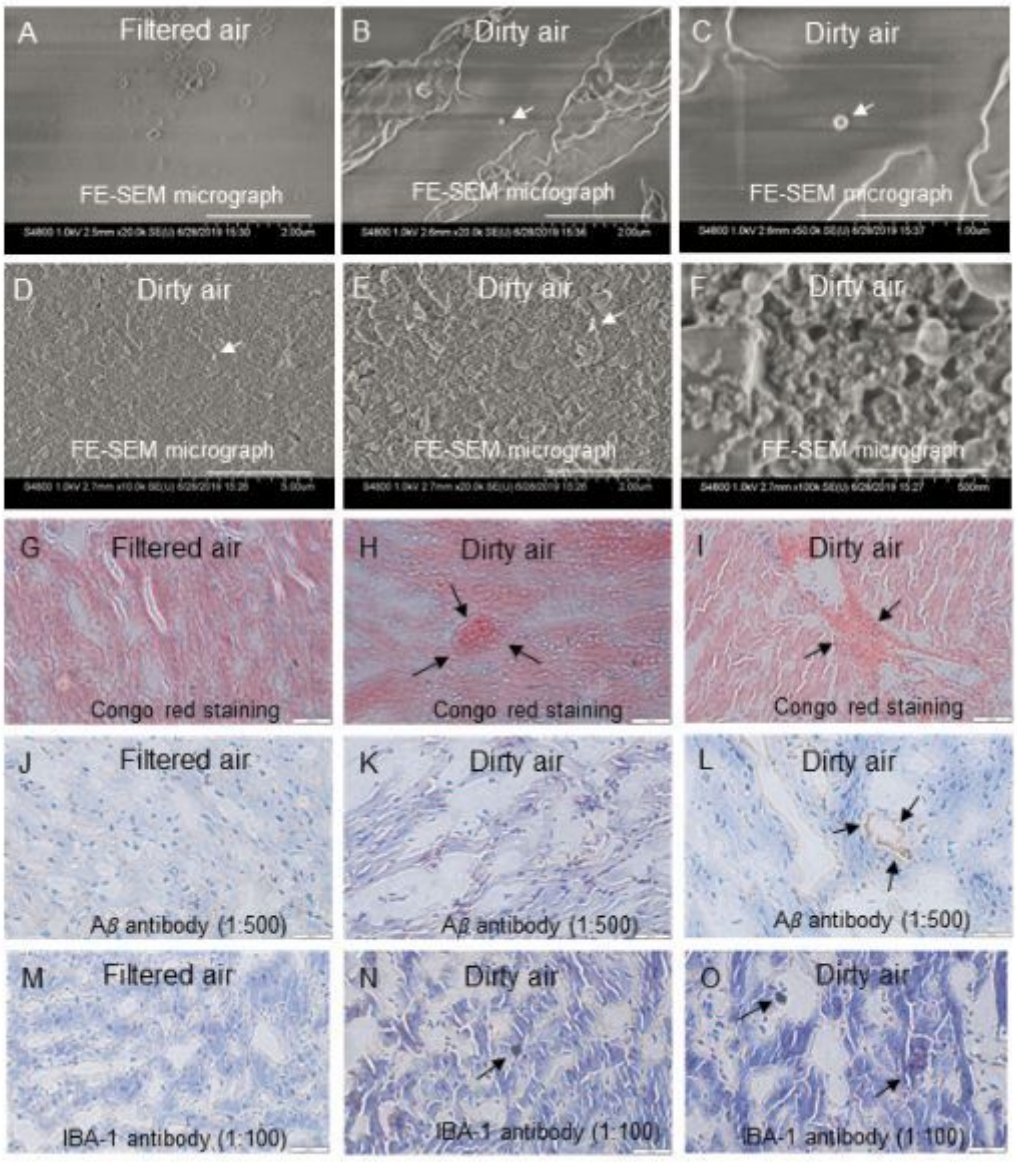

Figure 3

Filed emission scanning electron microscopy of heart tissues. (**A**) Heart tissues from filtered air showed no abnormality, whereas (**B** and **C**) heart tissue from dirty air exposure group showed $PM_{2.5}$ particles, (**D** and **E**) amyloid deposit, and (**F**) tissue damage. Histopathological evaluation by Congo red staining, (**G**) heart tissues from filtered air showed no abnormality, whereas (**H** and **I**) heart tissue from the dirty air showed amyloid deposition. Immunohistochemistry with Aβ antibody (1:500), (**J**) from heart of filtered air showed no abnormality, whereas (**K** and **L**) heart tissue from dirty air showed amyloid deposits. Immunohistochemistry with IBA-1 antibody (1:100), (**M**) heart tissues from filtered air showed no abnormality, whereas (**N** and **O**) heart tissue from dirty air showed inflammation. Magnification (**A, B** and **E**) 20k, scale bar: 2 µm. Magnification (**C**) 50k, scale bar 1 µm. Magnification (**D**) 10k, scale bar: 5 µm. Magnification (**F**) 100k, scale bar 500nm. Magnification (**G** to **O**) 40X, Scale bar: 500 µm.

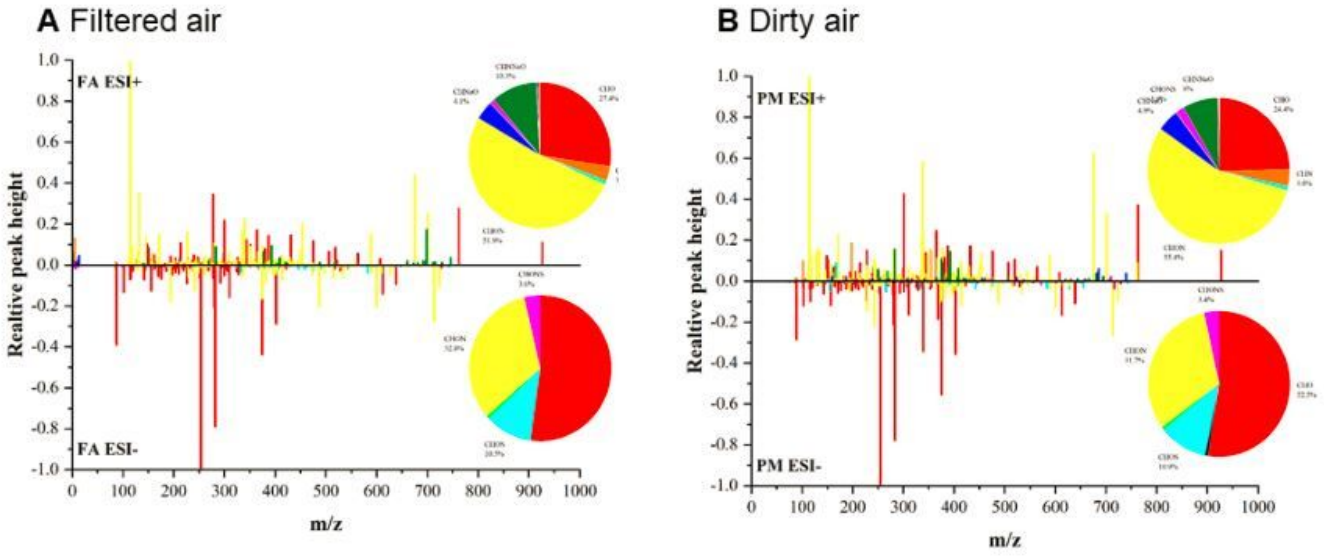

Figure 4

Legend not included with this version.

Supplementary Files

This is a list of supplementary files associated with this preprint. Click to download.

- FigureS1.tif

- SupplementaryMaterial.docx